International Journal of Mechanical Sciences 201 (2021) 106459

Contents lists available at ScienceDirect

International Journal of Mechanical Sciences

journal homepage: www.elsevier.com/locate/ijmecsci

High-velocity impact on composite sandwich structures: A theoretical model

L. Alonso [a], A. Solis [b,*]

[a] Department of Chemical Technology, Energy and Mechanics, Rey Juan Carlos University, C/Tulipán s.n., 28933, Spain
[b] Department of Mechanical Engineering and Industrial Design, University of Cádiz, Avda. de la Universidad de Cádiz 10, Puerto Real, 11519, Cádiz, Spain

ARTICLE INFO

Keywords:
Energy-absorption
Foam
Analytical modelling
High-velocity impact

ABSTRACT

A theoretical energy-based model to capture the ballistic response of sandwich structures made of composite material peels and a crushable foam core was developed. The model was based on the wave propagation theory and it was split in six stages with their corresponding energy-absorption mechanisms. The division of the stages was based on the physical interpretation of the perforation process involving reasonable hypotheses and simplifications. The energy-absorption was analysed at velocities below, near and above the ballistic limit within all the stages showing the general trends in terms of their relative importance. The time and velocity at each stage was separately analysed within a wide range of velocities in order to see the stage contribution to the energy-absorption. The model was validated against experimental results obtained in the literature showing a good agreement in terms of the impact-residual velocity curve.

1. Introduction

Composite materials are used in different structural applications because of their good mechanical properties. The main attraction of these materials is the low density compared to the traditional engineering materials such as steel or aluminium. These characteristics allow for the reduction of costs [9,12,13,16,17,29,46], which is an important requirement in any kind of industry. In general, composites can be used in such industries as aerospace, maritime or transport where they may be subjected to impulsive loads during their service life. In this context, laminates are a very common typology which implies several effects that may cause structural weakening such as free-edge interlaminar stresses [11,18] that vary depending on the stacking sequence or ply-orientation [49]. In addition, the operation and manufacture of such structures involve the presence of notches and holes that produces stress intensification and, hence, failure mechanisms as delamination [34,51]. In this sense, the determination of the presence of affected areas by the mentioned mechanisms has led to make efforts in proposing models based on the continuum mechanics [32], capable of predicting matrix damage, debonding of fiber and even fibre failure [41]. Woven laminates are also used to strengthen more complex structures in order to accomplish with all the structural requirements. Specifically, sandwich structures made of peels of composite materials and a lightweight core are used to manufacture components in aerospace and maritime applications in which compression and crushable loads are important [27,28,30]. In these applications, high-velocity impacts is a common scenario [4,21,22,54,55]. Consequently, the study of the ballistic performance of sandwich structures is a hot topic for researchers and engineers who look for design improvements in terms of safety and cost reduction.

There are different approaches to tackle the high-velocity impact phenomenon on sandwich structures: experimental, analytical and numerical. Every methodology has their advantages and inconveniences. Analytical and theoretical approaches are less expensive not only regarding to direct but to computational costs. The main advantage of analytical models is the quick estimation they can provide in terms of important aspects such as the ballistic limit using less resources than other methodologies [6,33,35–38,40]. Reyes Villanueva and Cantwell [44] carried out experiments to determine the ballistic limit in sandwich structures made of woven and unidirectional E/glass fibre peels and aluminium core. Ramadhan et al. [43] performed high-velocity impact tests on sandwich structures based on Kevlar-29 fibre/epoxy resin combined with aluminium in different stacking sequences and compared the results with a finite element model developed in Ansys obtaining a good agreement. Iváñez et al. [27] developed a finite element model to compare the ballistic response of sandwich plates made of E-glass fibre polyester facesheets and a crushable foam, which captured well the experimental results [8]. Regarding numerical and experimental studies of high-velocity impact on sandwich structures, less models are available [1,5,7,15,23,24,28,39,47,52].

* Corresponding author.
E-mail addresses: luis.alonso.sanjose@urjc.es (L. Alonso), alberto.solis@uca.es (A. Solis).

https://doi.org/10.1016/j.ijmecsci.2021.106459
Received 17 March 2021; Received in revised form 13 April 2021; Accepted 13 April 2021
Available online 21 April 2021

There are a relevant number of studies regarding numerical modelling of impact on sandwich structures [10,31,43,53]. Nevertheless, literature is less extensive regarding analytical models for high-velocity impact on sandwich structures. Hoo Fatt and Sirivolu [26] developed an analytical model based on the wave propagation theory to calculate the ballistic response of sandwich structures with crushable foams impacted by a hemispherical-nose cylindrical projectile. This model is divided into different stages depending on the distance reached by the through-thickness waves and considers different failure and deformation mechanisms using the Lagrangian method. Hoo Fatt and Park [25] also developed dynamic models for low-velocity impact on composite sandwich panels based on the phenomenon of indentation using the Lagrangian method. Feli and Namdari-Pour [14] formulated an analytical model for composite sandwich panels made of composite peels with honeycomb core subjected to high-velocity impact. The formulation is divided into three stages that take into account the different perforation processes and the first stage is based on the wave propagation theory. Energy-absorption mechanisms such as deformation of fibres, core crushing and kinetic energy transfer are considered. Reyes Villanueva and Cantwell [44] used a ballistic limit model to study sandwich structures based on plain composite and fibre-metal laminate (FML). This perforation model is based on the comparison of the resistive pressures generated in the structure to the failure stresses of the material in different directions. Analytical models can also be used to analyse interactions between different effects such as plastic bending or shear stresses and their consequences regarding the projectile indentation in the facesheet or internal core [42]. Moreover, the study of interesting effects as buckling can be undertaken using analytic perspectives, enabling the design of composite blades for wind turbines [50]. Another example may be the through-thickness thermal conductivity of each sandwich component including the foam core, facesheet and the bonding elements, which constitute phenomena of extraordinary complexity that can be also tackled using analytical models [45].

The gap regarding analytical models for sandwich structures subjected to high-velocity impact found in the literature has motivated this work. A new energy-based theoretical model for predicting the ballistic response of sandwich structures made of woven composite plates and crushable foams is presented. The model is based on the wave propagation theory and it is split into six stages, each one with their corresponding energy-absorption and failure mechanisms. The first and sixth stages are based on previous models developed by the authors [2,3] and the stages involving the foam behaviour are formulated using novel physically motivated hypotheses. The model is validated against experimental results obtained from the literature and interesting conclusions are obtained in terms of the energy-absorption contributions of the stages and the role they play.

2. Theoretical model

This section includes a detailed exposition of the proposed model to describe the behaviour of sandwich composite structures subjected to high-velocity impact. Such structures are manufactured with the assembly of two composite peels and a crushable foam core in between. The impact process takes into account several energy-absorption mechanisms which absorb the kinetic energy of the impactor. The entire process occurs in six different stages taking place sequentially with the projectile trajectory. The model is split into the mentioned stages, making a correspondence with the physics involved.

In the first subsection, the sandwich structure is described by means of the parameters used in the model, which allows to characterise the peels as well as the foam core. In the second subsection, the phase velocities of the different wave movements involved are determined using the expressions of the wave theory. The foam region affected by the plastic and transverse waves is also modelled by considering different possibilities. The third subsection exposes the hypotheses taken into account in order to state the stages described in the latest six subsections.

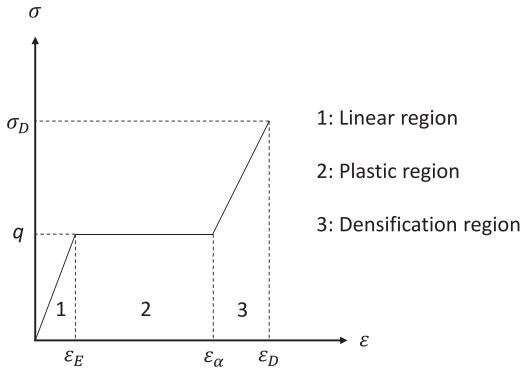

Fig. 1. Regular constitutive behaviour of an isotropic PVC crushable foam in terms of the strain versus stress curve and definition of the characteristic regions: linear-elastic (1), plastic (2) and densification (3).

2.1. Characterisation of the constituents

Both peels are woven E-glass/polyester laminates while the core is a PVC crushable foam. Note that the mechanical properties presented in Table 1 are dynamic values. The dynamic properties of the E-glass fibre at high strain rates used in the theoretical model are estimated from the static properties obtained in the tests taking into account the relations proposed by Harding and Ruiz [19], Harding and Welsh [20]. The high-strain rate correction factors for the failure limits and for the shear and Young's moduli are estimated at 3 and 1.5 respectively. All the parameters used are listed in Table 1:

The first composite plate is assumed to have a behaviour similar to the one proposed by Alonso et al. [3] for thick woven laminates. Even though the front laminate is thin, the foam and the back laminate provide an extra resistance in the through-thickness direction preventing the front laminate from bending. This hypothesis is based on experimental observations [27,28]. Due to these boundary conditions, the energy-absorption mechanisms considered for this laminate are: compression, tensile failure of fibres, shear plugging, kinetic energy transfer to the facesheet, matrix cracking and delamination. In this model, the main variable used to describe the penetration process is the geometric position of the projectile from the impact surface of the front plate. When the compressive out-of-plane failure strain is reached, the front laminate fails. After composite failure, a plug of material is formed. This plug is pulled up by the projectile. The friction between both bodies once failure has occurred is considered negligible because of the short laminate thickness.

On the other hand, the back composite plate is assumed to behave as a thin laminate as proposed by Alonso et al. [2]. In that work, a phenomenological function $k(t, v(t))$ which depends on the flexural rigidity, is defined to take into account the velocity of the laminate due to bending effects (Eq. (55)). Therefore, the effects cause by bending are considered. Once again, this hypothesis is based on experimental observations [27,28]. In this model, the relevant variable is the relative displacement between the projectile and the position of the first impacted facesheet of the back plate. Since thin laminate behaviour is assumed, the energy absorption mechanisms considered for this laminate are: kinetic energy transfer to the facesheet, elastic deformation of fibres, tensile failure of fibres, delamination and matrix cracking. The stop condition is met when the relative displacement between the projectile and the facesheet equals the laminate thickness.

The main novelty of this work is the model proposed for the foam core. The considerations assumed allow for the determination of the sandwich structure ballistic limit. The model gives information about the time spent by the projectile within each stage and the amount of energy absorbed by each energy-absorption mechanism. The foam behaviour can be described in the strain versus stress curve shown in Fig. 1

Table 1
Summary of the parameters used in the theoretical model.

Parameter	Nomenclature	Value
Projectile		
Projectile Diameter	ϕ_p	7.5 [mm]
Projectile Density	ρ_p	7809 [kg m^{-3}]
Impact Velocity	v_i	[m s^{-1}]
E-glass Fibre Laminate		
Laminate Thickness	e_t	3 [mm]
Laminate Density	ρ_l	1980 [kg m^{-3}]
In-Plane Young's Modulus	E	15.2 [GPa]
Compressive Out-of-Plane Young's Modulus	E_c	6.75 [GPa]
In-Plane Failure Strain	ε_r	0.0725
Compressive Out-of-Plane Failure Strain	ε_{rc}	0.217
Out-of-Plane Failure Shear Stress	S_{SP_l}	201.42 [MPa]
In-plane Failure Stress	σ_r	1.102 [GPa]
Absorbed Energy Density by Matrix Cracking	E_{MT}	10^6 [J m^{-3}]
Critical Dynamic-Strain Energy-Release Rate in Mode II	G_{IICD}	3000 [J m^{-2}]
Yarn Width	B	5 [mm]
Stress Wave Transmission Factor	b	0.9
Poisson's Ratio	ν	0.16
Constant	c	0.25 [N m]$^{-1/6}$
Shape Factor of Delamination	α_{DL}	1
Shape Factor of Matrix Cracking	α_{MC}	1
Foam		
Yield Stress	q	2.63 [MPa]
Maximum Elastic Foam Strain	ε_E	0.0302
Plastic Limit Strain	ε_α	0.5115
Densification Limit Strain	ε_D	0.6264
Densification Limit Stress	σ_D	3.549 [MPa]
Density	ρ_f	130 [kg m^{-3}]
In-Plane Young's Modulus	E_f	87 [MPa]
In-Plane Poisson's Modulus	ν_f	0.32
Out-of-Plane Failure Shear Stress	S_{SP_f}	2 [MPa]
Thickness	e_e	30 [mm]

assuming the material is isotropic. Note that three different zones can be distinguished in the mentioned curve. The first one corresponds to the foam elastic behaviour limited by the yield stress, q, and the maximum elastic strain, ε_E, respectively. Then, an ideal plastic deformation where stress remains constant is assumed up to ε_α. From this point, a linear densification process takes place up to the maximum densification stress, σ_D, and strain, ε_D, where the complete failure occurs.

2.2. Wave theory

The foam model proposed is based on the wave theory described by Smith et al. [48] and, consequently, considers independent wave movements. The transverse, $C_{V_{t_l}}$, and through-thickness, $C_{V_{x_l}}$, wave velocities within the laminates are given by:

$$C_{V_{t_l}} = \sqrt{(1+\varepsilon_r)\frac{\sigma_r}{\rho_l}} - \sqrt{\frac{E}{\rho_l}}\varepsilon_r \tag{1}$$

$$C_{V_{x_l}} = \sqrt{\frac{E_c}{\rho_l}} \tag{2}$$

where ρ_l, σ_r and ε_r are the laminate density and the in-plane failure stress and strain while E and E_c are the in-plane and compressive out-of-plane Young's modulus respectively. Regarding the foam, given that the compression elastic wave can be neglected when the foam particles maximum velocity in the elastic zone is small compared to the projectile velocity [26], only the plastic wave is needed to be considered to measure the energy absorbed by compression. The phase velocity of the compression plastic wave, C_p is:

$$C_p = \sqrt{\frac{(\sigma_D - q)}{\rho_f \varepsilon_D}} \tag{3}$$

where ρ_f is the foam density, σ_D is the densification limit stress, q is the yield stress and ε_D is the densification limit strain. In addition, the wave responsible for the foam acceleration is the transverse wave that travels with a phase velocity, $C_{V_{t_f}}$, by Smith et al. [48]:

$$C_{V_{t_f}} = \sqrt{(1+\varepsilon_E)\frac{q}{\rho_f}} - \sqrt{\frac{E_f}{\rho_f}}\varepsilon_E \tag{4}$$

where E_f is the in-plane foam Young's modulus and ε_E is the maximum elastic foam strain. This approach considers that the expansion of the transverse perturbation has a moving boundary that spreads away radially from the impact point up to a distance $C_{V_{t_f}} t$ (the origin of t is referred to the instant when the plastic wave reaches the foam). Under the projectile, the plastic wave front advances a distance $C_p t$ in the through-thickness direction along with the lateral perturbation. This lateral perturbation diminishes linearly from a radial value equal to $C_{V_{t_f}} t$ on the front face of the foam to zero at a distance equal to $C_p t$ right underneath the projectile. The region affected by the two mentioned wave fronts is represented in Fig. 2. Depending on the instant t, the region can be a cone or a truncated cone respectively. If $t \leq \frac{e_e}{C_p}$ (being e_e the foam thickness), the situation is represented in Fig. 2(a). Otherwise, the region affected by the plastic wave is a truncated cone (Fig. 2(b)). This last situation occurs when the plastic wave front reaches the second composite laminate. Hence, the account of the energy absorbed by compression in the foam implies the determination of the volume of the region affected by compression according to the two possibilities shown in Fig. 2 (being e_t is the peels thickness). Consequently, the volume V_c of the region affected by compression is:

$$V_c(t) = \begin{cases} \frac{\pi C_p C_{V_{t_f}}^2}{3} t^3, & \text{if } t \leq \frac{e_e}{C_p} \\ \frac{\pi C_p (C_{V_{t_f}})^2}{3}\left[t^3 - (t - \frac{e_e}{C_p})^3\right], & \text{if } t > \frac{e_e}{C_p} \end{cases} \tag{5}$$

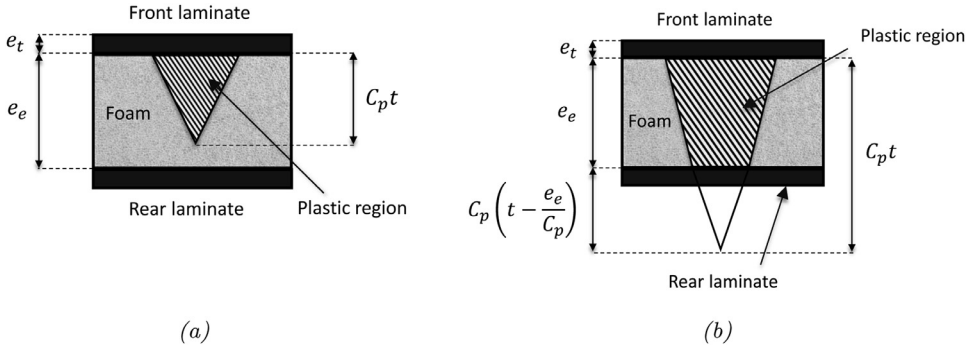

Fig. 2. Representation of the foam region affected by the plastic wave (striped area), marked out by the cone or the truncated cone defined by the growth of the transverse ($C_{V_{tf}}t$) and the plastic ($C_p t$) waves, accounting for the two admissible possibilities: (a) Case $t \leq \frac{e_e}{C_p}$, (b) Case $t > \frac{e_e}{C_p}$.

2.3. Description of the stages and hypotheses

The six stages considered in this model are independent, so that the outputs of a previous stage are the inputs for the next. The first stage starts when the projectile reaches the front plate. From this moment on, several waves are transmitted through the plate in different directions and different energy-absorption mechanisms are considered according to the thick woven laminates theory hypotheses formulated by Alonso et al. [3]. This stage ends when the complete compression failure of the laminate takes place. At that moment, a plug with a certain kinetic energy is formed. Since there are not external forces, an instantaneous linear momentum transfer to the plug is assumed to take place in the second stage. The unique body formed by the composite plug and the projectile starts to penetrate the foam in the third stage until the foam fails by shear forces. In this stage, compression and shear energy-absorption mechanisms are considered. Once the foam has failed by shear, the plug formed in the foam experiments a densification process during the fourth stage. This stage ends when the foam reaches a deformation equal to ε_D. In the fifth stage, an instantaneous linear momentum transfer is assumed to calculate the final velocity to the body conformed by the projectile and both plugs (laminate and foam). The last stage consists on the penetration into the back composite peel which behaves as a thin woven laminate according to the hypotheses also considered by Alonso et al. [2]. The relative displacement between the projectile and the front face movement reaching the back facesheet thickness is the stop condition of the entire process.

As described above, the first and sixth stages are described using the hypotheses and ideas proposed by Alonso et al. [2,3], so those hypotheses are also considered for the first and last stage in this work. Additionally, some hypotheses regarding the foam are assumed:

- The core of the sandwich structure is considered isotropic.
- Since $\frac{\rho_f}{\rho_p}, \frac{\rho_f}{\rho_l} << 1$ (being ρ_p and ρ_l the projectile and laminates density respectively[1]), the kinetic energy transfer by the projectile to the foam is neglected. Hence, the only energy-absorption mechanisms considered are compression and shear.
- Two different waves are considered in the foam: a plastic compression wave and a transverse wave. All wave velocities remain constant during the impact process.
- The impact process is divided into the six stages described below.
- The first stage ends when the complete failure of the front laminate takes place.
- At the end of the second and fifth stages, it is assumed that a unique body is formed by the projectile and different material plugs.
- The third stage ends when the complete shear failure of the foam takes place.
- The fourth stage ends when the foam densification strain reaches ε_D.
- The energy absorbed by heat transfer and friction between the projectile and the foam is assumed to be negligible.

In the following sections, all the stages are fully described.

2.4. Stage 1

The first stage is formulated in terms of an instantaneous energy balance. The initial kinetic energy of the projectile, E_0, is equal to the kinetic energy of the projectile, $E_p(t)$, plus the energy absorbed by the energy-absorption mechanisms until the current instant t, $E_{AB}(t)$:

$$E_0 = E_p(t) + E_{AB}(t) \tag{6}$$

where $E_{AB}(t)$ is defined as:

$$\begin{aligned} E_{AB}(t) = {} & E_f(t) + E_{C1}(t) + E_{C2}(t) + E_{TF}(t) \\ & + E_{CL}(t) + E_{SP}(t) + E_{MC}(t) + E_{DL}(t) \end{aligned} \tag{7}$$

where $E_f(t)$ is the energy absorbed by compression in the foam, $E_{C1}(t)$ and $E_{C2}(t)$ are the energy absorbed by compression in the laminate, $E_{TF}(t)$ is the energy absorbed by tensile failure of fibres, $E_{CL}(t)$ is the energy absorbed by kinetic energy transfer, $E_{MC}(t)$ is the energy absorbed by matrix cracking and $E_{DL}(t)$ is the energy absorbed by delamination. All these mechanisms and their expresions are fully explained in Alonso et al. [3] except for $E_f(t)$ that will be shown up next.

To account for the energy absorbed by compression in the foam, three possibilities arises depending on the distance travelled by the through-thickness and plastic waves: if[2] $t \leq \frac{e_t}{C_{V_{x_l}}}$, the energy absorbed by this mechanisms is zero, else if $\frac{e_t}{C_{V_{x_l}}} < t \leq \frac{e_t}{C_{V_{x_l}}} + \frac{e_e}{C_p}$ the energy absorbed is the energy below the stress-strain curve[3] shown in Fig. 1 times the volume of the cone (Fig. 2(a)), else if $t > \frac{e_t}{C_{V_{x_l}}} + \frac{e_e}{C_p}$ the energy absorbed by compression in the foam is the energy below the stress-strain curve shown in Fig. 1 times the volume of the truncated cone (Fig. 2(b)):

$$E_f(t) = \begin{cases} 0, & \text{if } t \leq \frac{e_t}{C_{V_{x_l}}} \\ \frac{\pi}{3} q\varepsilon_\alpha C_p C_{V_{tf}}^2 \left(t - \frac{e_t}{C_{V_{x_l}}}\right)^3, & \text{if } \frac{e_t}{C_{V_{x_l}}} < t \leq \frac{e_t}{C_{V_{x_l}}} + \frac{e_e}{C_p} \\ \frac{\pi}{3} q\varepsilon_\alpha C_p C_{V_{tf}}^2 \left[\left(t - \frac{e_t}{C_{V_{x_l}}}\right)^3 - \left(t - \frac{e_t}{C_{V_{x_l}}} - \frac{e_e}{C_p}\right)^3\right], & \text{if } t > \frac{e_t}{C_{V_{x_l}}} + \frac{e_e}{C_p} \end{cases} \tag{8}$$

Note that the expressions to calculate the energy absorbed by kinetic energy transfer and compression [3] are replaced for the following ones if the through-thickness wave reaches the laminate before laminate failure occurs $\left(t > \frac{e_t}{C_{V_{x_l}}}\right)$:

$$E_{CL}(t) = \frac{\pi \rho_l e_t}{24} v(t)^2 \phi(x)^2 \tag{9}$$

$$E_{C1}(t) = \frac{\pi}{8} e_t E_c \varepsilon_{rc}^2 \phi(x)^2 \tag{10}$$

[1] Some reference values are $\frac{\rho_f}{\rho_p} \sim \frac{1}{100}$, $\frac{\rho_f}{\rho_l} \sim \frac{1}{20}$

[2] t is referred to the instant the projectile reaches the laminate front face

[3] This energy will be estimated by $q\varepsilon_\alpha$ according to Eq. (23).

Derivation of Eq. (6) with respect to time, gives the non-linear second-order differential equation governing the first stage:

$$a(t) = \begin{cases} \dfrac{g(t,x(t),v(t)) - h(t)(t,v(t))v(t) - f(t,x(t)) - p(t) - \frac{\pi}{24}\rho_l C_{v_{x_l}}\left[2v(t)^3\phi(x)\frac{d\phi}{dx}t + v(t)^2\phi(x)^2\right]}{m_p v(t) + \frac{\pi}{12}\rho_l C_{v_{x_l}} v(t)\phi(x)^2 t} & \text{if } t \le \dfrac{e_t}{C_{V_{x_l}}} \\ \dfrac{g(t,x(t),v(t)) - h(t)(t,v(t))v(t) - f(t,x(t)) - p(t) - \frac{\pi}{12}\rho_l e_t v(t)^3\phi(x)\frac{d\phi}{dx}}{m_p v(t) + \frac{\pi}{12}\rho_l e_t v(t)\phi(x)^2} & \text{if } t > \dfrac{e_t}{C_{V_{x_l}}} \end{cases} \tag{11}$$

Both equations are subjected to the following initial conditions:

$$x(0) = 0 \qquad v(0) = V_i \tag{12}$$

In order to obtain Eq. (11), the following functions are defined to operate easier:

$$h(t,v(t)) = \frac{d}{dt}\left[E_{TF}(t) + E_{SP}(t)\right]\frac{1}{v(t)} \tag{13}$$

$$g(t,x(t),v(t)) = \begin{cases} -\dfrac{d}{dt}[E_{DL}(t) + E_{MC}(t)], & \text{if } t \le \dfrac{\phi(x)}{2C_{V_{t_l}}} \\ -\dfrac{d}{dt}[E_{C2}(t) + E_{DL}(t) + E_{MC}(t)], & \text{if } t > \dfrac{\phi(x)}{2C_{V_{t_l}}} \end{cases} \tag{14}$$

$$f(t,x(t)) = \frac{dE_{C1}(t)}{dt} \tag{15}$$

$$p(t) = \frac{dE_f(t)}{dt} \tag{16}$$

This stage finishes when the failure condition given by Eq. (17) is met. At this moment, the velocity of the projectile is the initial velocity for the second stage.

$$x(t) = e_t\varepsilon_{rc} \tag{17}$$

From this point, the parameters t_{f_1} and $V_{f_1} = V_{i_2}$ are defined as the end time of the first stage and the initial velocity of the second stage respectively.

2.5. Stage 2

When the first stage finishes, a plug of material is formed. In the second stage a perfect instantaneous inelastic shock is assumed between the projectile and the plug formed. After the shock, the two bodies moves with the same velocity. Conservation of linear momentum provides a scalar equation from which the final velocity of the whole can be obtained, $V_{f2} = V_{i3}$:

$$p_{1l} + m_p V_{i_2} = (m_p + m_l)V_{f_2} \tag{18}$$

where m_p is the projectile mass, m_l is the plug mass, p_{1l} is the linear momentum of the plug an instant before failure and can be calculated assuming a linear profile of velocities between the point in contact with the projectile and the distance travelled by the through-thickness wave across the laminate as explained in Alonso et al. [3]:

$$m_p = \frac{\pi}{6}\rho_p\phi_p^3 \tag{19}$$

$$m_l = \frac{\pi}{4}\rho_l e_t\phi_p^2 \tag{20}$$

$$p_{1l} = \frac{\pi}{8}\rho_l C_{V_{x_l}} V_{i_2}{\phi_1}^2 t_{f_1} \tag{21}$$

where ϕ_p is the projectile diameter and ϕ_1 is the indented diameter of the projectile when the first stage ends. Therefore, the initial velocity of the third stage is given by:

$$V_{i_3} = \frac{p_{1l} + m_p V_{i_2}}{m_p + m_l} \tag{22}$$

2.6. Stage 3

In this section, the penetration process of the body formed by the projectile and the composite plug in the foam core is described. As already stated, two different energy-absorption mechanisms are taken into account: plastic compression and shear.

2.6.1. Energy absorbed by plastic compression in the foam

The energy absorbed by compression, E_{Cf3}, in the third stage may be calculated as the energy below the compressive stress-strain curve in the thickness direction times the volume V_c of the affected region.

$$E_{Cf3}(t) = V_c(t)\int_0^{\varepsilon_\alpha}\sigma(\varepsilon)\,d\varepsilon \approx V_c(t)q\varepsilon_\alpha \tag{23}$$

where the area below the stress-strain curve in the plastic region is estimated by $q\varepsilon_\alpha$ and the volume affected, V_c (represented by the striped areas in Fig. 3) must be calculated depending on the situation and the region previously affected by the plastic compression wave at the starting instant t_{f_1} of the third stage. If $t_{f_1} = t_{f_2} \ge \frac{e_t}{C_{V_{xl}}} + \frac{e_e}{C_p}$, the initial plastic compression wave front has traveled through the entire foam thickness (case shown in Fig. 3(e)). On the other hand, if $t_{f_1} > \frac{e_t}{C_{V_{xl}}}$ and $t_{f_1} < \frac{e_t}{C_{V_{xl}}} + \frac{e_e}{C_p}$ the initial plastic compression wave front is located somewhere in the foam thickness (Fig. 3(c) and (d)). Otherwise, the initial compression wave front has not reached the foam yet, therefore, the last cases occur when $t_{f_1} \le \frac{e_t}{C_{V_{x_l}}}$ (cases shown in Fig. 3(a) and (b)). Additionally, depending on the value of t (t is measured from the initial instant t_{f_1} of the third stage), the region affected by plastic compression can acquired different shapes.

If $t_{f1} \ge \frac{e_t}{C_{V_{xl}}} + \frac{e_e}{C_p}$, the energy absorbed by plastic compression in the foam is (the volume of the region affected is represented by stripes in Fig. 3(e)):

$$E_{Cf3}(t) = \frac{\pi}{3}C_p(C_{V_{tf}})^2 q\varepsilon_\alpha\left[\left(t_{f1} - \frac{e_t}{C_{V_{xl}}} + t\right)^3 - \left(t_{f1} - \frac{e_t}{C_{V_{xl}}} + t - \frac{e_e}{C_p}\right)^3 - \left(t_{f1} - \frac{e_t}{C_{V_{xl}}}\right)^3 + \left(t_{f1} - \frac{e_t}{C_{V_{xl}}} - \frac{e_e}{C_p}\right)^3\right] \tag{24}$$

Conversely, if $t_{f_1} > \frac{e_t}{C_{V_{xl}}}$, $t_{f1} < \frac{e_t}{C_{V_{xl}}} + \frac{e_e}{C_p}$ and $t + t_{f1} - \frac{e_t}{C_{V_{xl}}} \le \frac{e_e}{C_p}$ the volume of the region affected represented in Fig. 3(c) leads to the following expression for the energy absorbed by compression:

$$E_{Cf3}(t) = \frac{\pi}{3}C_p(C_{V_{tf}})^2 q\varepsilon_\alpha\left[\left(t_{f1} - \frac{e_t}{C_{V_{xl}}} + t\right)^3 - \left(t_{f1} - \frac{e_t}{C_{V_{xl}}}\right)^3\right] \tag{25}$$

Analogously, if $t_{f_1} > \frac{e_t}{C_{V_{xl}}}$, $t_{f1} < \frac{e_t}{C_{V_{xl}}} + \frac{e_e}{C_p}$ and $t + t_{f1} - \frac{e_t}{C_{V_{xl}}} > \frac{e_e}{C_p}$, the volume of the region affected is represented in Fig. 3(d) and thus

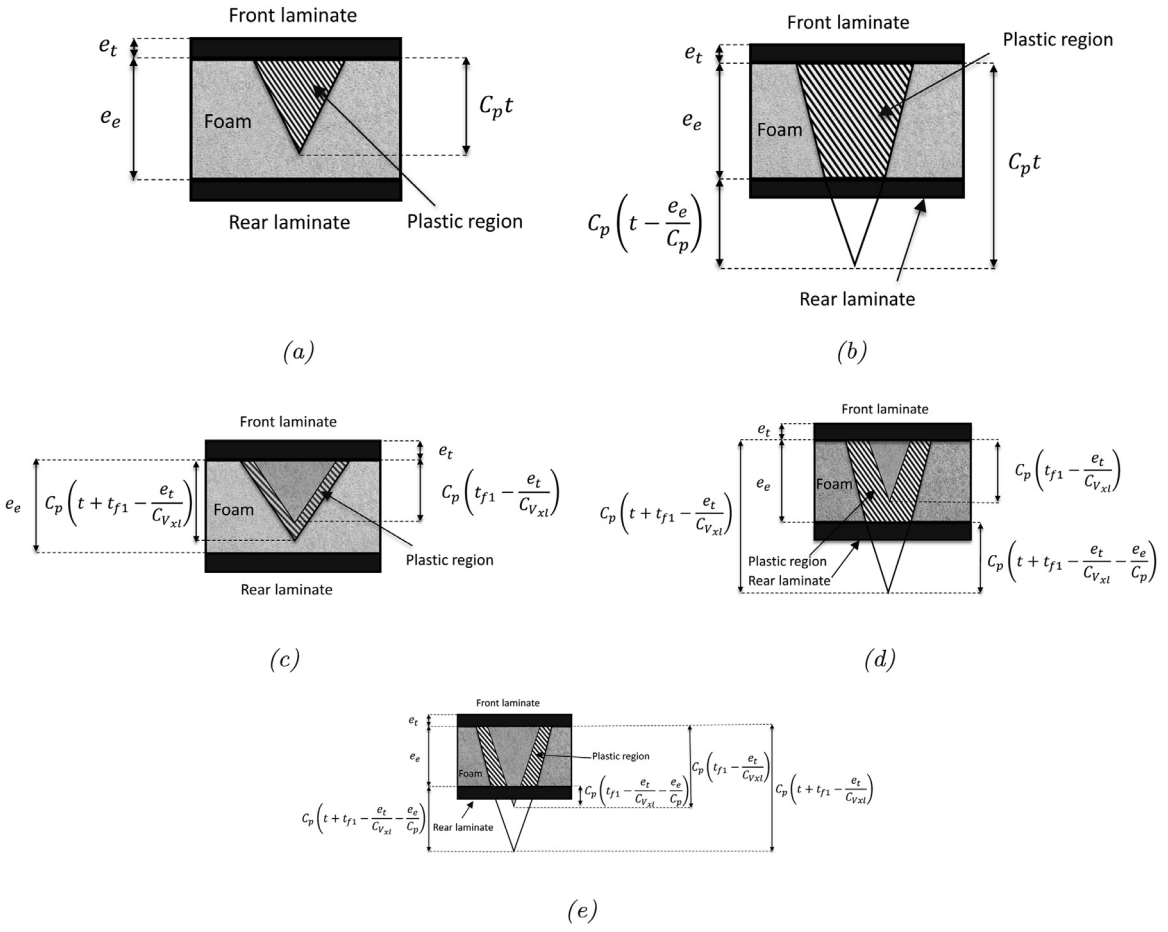

Fig. 3. Representation of the foam region affected by the plastic wave from the beginning of the third stage on, defined by the body of revolution delimited by the striped area and considering all the possible situations depending on the impact and wave velocities: (a) $t_{f1} \leq \frac{e_t}{C_{V_{xl}}} \cup t \leq \frac{e_e}{C_p}$, (b) $t_{f1} \leq \frac{e_t}{C_{V_{xl}}} \cup t > \frac{e_e}{C_p}$, (c) $t_{f1} > \frac{e_t}{C_{V_{xl}}} \cup t_{f1} < \frac{e_t}{C_{V_{xl}}} + \frac{e_e}{C_p} \cup t + t_{f1} - \frac{e_t}{C_{V_{xl}}} \leq \frac{e_e}{C_p}$, (d) $t_{f1} > \frac{e_t}{C_{V_{xl}}} \cup t_{f1} < \frac{e_t}{C_{V_{xl}}} + \frac{e_e}{C_p} \cup t + t_{f1} - \frac{e_t}{C_{V_{xl}}} > \frac{e_e}{C_p}$, (e) $t_{f1} \geq \frac{e_t}{C_{V_{xl}}} + \frac{e_e}{C_p}$.

the energy absorbed may be expressed as:

$$E_{Cf3}(t) = \frac{\pi}{3} C_p (C_{V_{tf}})^2 q \varepsilon_\alpha \left[\left(t_{f1} - \frac{e_t}{C_{V_{xl}}} + t \right)^3 - \left(t_{f1} - \frac{e_t}{C_{V_{xl}}} \right)^3 - \left(t_{f1} - \frac{e_t}{C_{V_{xl}}} + t - \frac{e_e}{C_p} \right)^3 \right] \tag{26}$$

Finally, if $t_{f1} \leq \frac{e_t}{C_{V_{xl}}}$ and $t \leq \frac{e_e}{C_p}$ or $t_{f1} \leq \frac{e_t}{C_{V_{xl}}}$ and $t > \frac{e_e}{C_p}$, the volumes affected by plastic compression are represented in Fig. 3(a) and (b) respectively. Consequently, the energy absorbed by plastic compression is respectively:

$$E_{Cf3}(t) = \frac{\pi}{3} C_p (C_{V_{tf}})^2 q \varepsilon_\alpha t^3 \tag{27}$$

$$E_{Cf3}(t) = \frac{\pi}{3} C_p (C_{V_{tf}})^2 q \varepsilon_\alpha \left[t^3 - \left(t - \frac{e_e}{C_p} \right)^3 \right] \tag{28}$$

2.6.2. Energy absorbed by shear plugging in the foam

In the modelling of this stage, a certain capacity of the foam to withstand shear stresses is considered. The unique body composed by the projectile and the composite plug in contact with the foam is responsible for these stresses. If the value of the shear stress transmitted to the foam exceeds the maximum shear strength of the material S_{SP_f}, the laminate will fail by shear plugging. Therefore, the energy absorbed by this mechanism can be calculated by multiplying the annular contact area by the maximum material shear stress in directions 13 and 23 and by the formed body displacement as follows:

$$E_{SP_f}(t) = \pi \phi_p e_e S_{SP_f} x(t) \tag{29}$$

where $x(t)$ is the position of the body conformed by the projectile and the composite plug respect to the front face of the foam as can be seen in Fig. 4. While the moving body is shown in grey, the dash line cylinder represents the projected area that will be affected by shear plugging as

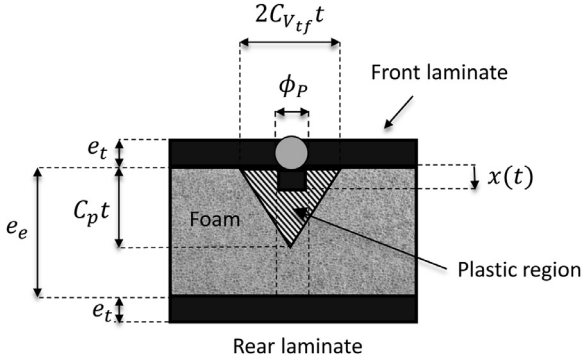

Fig. 4. Scheme of the impact phenomenon at a generic instant of time in the third stage when the composite material plug has already been formed and travels alongside the projectile. The foam absorbs energy by compression and shear plugging with the coupled through-thickness movement of the two bodies.

the body goes through. The cone indicates the volume affected by plastic compression.[4]

2.6.3. Energy balance and governing equation of the third stage

In order to obtain the governing equation that describes the advance of the body in terms of $x(t)$ in the third stage, an energy balance is formulated. This balance consists of applying the conservation of energy. The kinetic energy of the body at the beginning of the third stage, E_{03}, is equal to the actual kinetic energy of the body, $E_p(t)$, plus the energy absorbed by compression and shear, $E_{AB_3}(t)$:

$$E_{03} = E_p(t) + E_{AB_3}(t) \tag{30}$$

$$E_p(t) = \frac{1}{2}(m_p + m_l)v(t)^2 \tag{31}$$

$$E_{AB_3}(t) = E_{Cf3}(t) + E_{SP_f}(t) \tag{32}$$

The differential equation governing this stage is obtained by deriving Eq. (30) with respect to time:

$$0 = \left(m_p + m_l\right)v(t)a(t) + \frac{dE_{Cf3}(t)}{dt} + \frac{dE_{SPf}(t)}{dt} \tag{33}$$

where $\frac{dE_{SP_f}(t)}{dt}$ is the shear energy absorption derivative with respect to t, which can be calculated as:

$$\frac{dE_{SP_f}(t)}{dt} = \pi\phi_p e_e S_{SP_f} v(t) \tag{34}$$

In order to obtain $\frac{dE_{Cf3}(t)}{dt}$, it is required to derive with respect to t in Eqs. (24)–(28) depending on the actual case as shown in Fig. 3. Substituting Eq. (34) in Eq. (33) and clearing $a(t)$, the governing equation is obtained:

$$\begin{aligned} a(t) &= -\frac{1}{(m_p+m_l)v(t)}\frac{dE_{Cf3}(t)}{dt} - \frac{\pi\phi_p e_e S_{SP_f}}{(m_p+m_l)} \\ x(0) &= 0 \\ v(0) &= V_{i_3} \end{aligned} \tag{35}$$

The stop condition for the second-order differential equation given in Eq. (35) is met when the maximum shear deformation is reached. This parameter can be approximated by $S_{SP_f} = \frac{E_f}{2(1+\nu_f)}\gamma_{13,23}$. In this approach, $\gamma_{13,23}$ is estimated by $2\frac{x(t)}{\phi_p}$. Taking all these considerations into account, the stop condition can be formulated in terms of $x(t) = X_{f_3}$ by:

$$X_{f3} = \frac{S_{SP_f}(1+\nu_f)\phi_p}{E_f} \tag{36}$$

When such condition is met, the actual velocity $V_{f3} = V_{i4}$ of the body is the initial condition of the next stage and the foam densification starts.

2.7. Stage 4

In this stage, the densification process represented in the last zone in Fig. 1 is mathematically described. The only energy absorbed in this stage is the area below the strain-stress curve times the foam volume affected by densification. Such energy and its derivative with respect to time can be expressed respectively as:

$$E_D(t) = q(\varepsilon - \varepsilon_\alpha)\frac{\pi}{4}\phi_p^2 e_e = q\frac{\pi}{4}\phi_p^2 x(t) \tag{37}$$

$$\frac{dE_D(t)}{dt} = q\frac{\pi}{4}\phi_p^2 v(t) \tag{38}$$

[4] This cone is a simplification of the affected plastic region made for clarity. The exact volume of the region affected by plastic compression in each step must be calculated by identification of the actual situation of those given in Fig. 3.

where the relative strain $(\varepsilon - \varepsilon_\alpha)$ is considered to be $\frac{x(t)}{e_e}$. The energy conservation equation is obtained again equaling the initial kinetic energy of the body at the beginning of the stage E_{04} to the actual kinetic energy $E_p(t)$ plus the energy absorbed by densification $E_D(t)$:

$$E_{04} = E_p(t) + E_D(t) \tag{39}$$

Deriving Eq. (39) with respect to time, the governing equation of this stage is obtained:

$$0 = (m_p + m_l)v(t)a(t) + \frac{dE_D(t)}{dt} \tag{40}$$

By replacing Eqs. (38) in (40) and clearing $a(t)$, a uniform accelerated movement equation is obtained:

$$a(t) = -q\frac{\pi}{4}\phi_p^2\frac{1}{(m_p + m_l)} = a \tag{41}$$

The stop condition is given by considering that the densification limit strain is reached. Hence, the position that implies the foam failure is:

$$X_{f4} = \varepsilon_D e_e - X_{f3} \tag{42}$$

By integration of Eq. (41) twice with respect to time and substitution of X_{f4}, the end time and velocity, t_{i5}, V_{i5}, at the end of densification process can be calculated respectively:

$$t_{i5} = -\frac{V_{i4}}{a} + \sqrt{\left(\frac{V_{i4}}{a}\right)^2 + \frac{2X_{f4}}{a}} \tag{43}$$

$$V_{i5} = at_{i5} + V_{i4} \tag{44}$$

When the strain ε_D is reached, the foam fails and a foam plug is formed and pulled up from the foam core. To determine the initial velocity in the sixth stage, a linear momentum balance is considered in the fifth stage.

2.8. Stage 5

Same as in the second stage just before failure, the unique body formed by the projectile and the composite plug moves with a certain linear momentum. In addition, some kinetic energy has been transferred to the foam. After failure, the new ensemble conformed by the projectile and both material plugs moves along with the same velocity. This linear momentum transfer is assumed to be instantaneous. Since in this stage there are no external forces, the conservation of linear momentum in the x-direction can be established in the next scalar equation:

$$(m_p + m_l)V_{i5} + p_e = (m_p + m_l + m_e)V_{i6} \tag{45}$$

where p_e is the linear momentum transmitted to the foam and m_e is the mass of foam plug that has been pulled up being:

$$p_e = \rho_f \int_{V_f} v(r)\, dV \tag{46}$$

$$m_e = \frac{\pi}{4}\phi_p^2 e_e \rho_f \tag{47}$$

where V_f is the affected foam volume and $v(r)$ is the foam particles velocity in the x-direction in each position. However, the linear momentum acquired by the foam p_e can be supposed to be of the order of $\sim \rho_f V_f V_{i5}$ before failure. Hence, it can be neglected as the ratios $\frac{\rho_f}{\rho_p}$, $\frac{\rho_f}{\rho_l}$ are much smaller than one. In balance terms, this aspect means that the linear momentum transferred to the foam is negligible with respect to the linear momentum of the body formed by the projectile and the composite plug.

Taking these aspects into account and clearing V_{i6} from Eq. (45), the initial velocity in the sixth stage is:

$$V_{i6} = \frac{(m_p + m_l)}{(m_p + m_l + m_e)} V_{i5} \tag{48}$$

2.9. Stage 6

Following the same procedure from the other stages an instantaneous energy balance is formulated. The initial kinetic energy of the projectile and plugs at the beginning of this stage, E_{06}, is equal to the kinetic energy of the projectile and plugs at any moment, $E_p(t)$, plus the energy absorbed by the energy-absorption mechanisms until this moment, $E_{AB_6}(t)$:

$$E_{06} = E_p(t) + E_{AB_6}(t) \tag{49}$$

$$E_p(t) = \frac{1}{2}(m_p + m_l + m_e)v(t)^2 \tag{50}$$

$$E_{AB_6}(t) = E_L(t) + E_{ED}(t) + E_{TF}(t) + E_{DL}(t) + E_{MC}(t) \tag{51}$$

where $E_L(t)$ is the kinetic energy transferred to the laminate, $E_{ED}(t)$ is the energy absorbed by elastic deformation of fibres, $E_{TF}(t)$ is the energy absorbed by tensile failure of fibres, $E_{MC}(t)$ is the energy absorbed by matrix cracking and $E_{DL}(t)$ is the energy absorbed by delamination. All these mechanisms and their expressions are fully explained in Alonso et al. [2]. Since this laminate is assumed to behave as thin a relative displacement between the laminate and the previous body (projectile plus the plugs), $\delta(t)$, is assumed to account for the penetration. The main difference respect to the model proposed by Alonso et al. [2] is that the geometry of the impactor is assumed to be cylindrical because the plugs penetrates first. Hence, the impactor diameter is assumed to be constant from the beginning with a value equal to the projectile diameter. The impactor mass is calculated as the sum of the projectile mass plus the plug masses.

Derivation of Eq. (49) with respect to time, gives the non-linear second-order differential equation governing the sixth stage:

$$\begin{aligned} a(t) = & \frac{g(t,x(t),v(t)) - h(t,v(t))v(t)}{(m_p+m_l+m_f)v(t) + \pi e_t \rho_l {C_{V_{t_l}}}^2 \left[t^2 k(t,v(t))^2 v(t) + \frac{2cD^{1/6}}{{V_{i6}}^2} \left(\frac{C_{V_{t_l}}}{e_t} \right)^{1/2} t^{5/2} k(t,v(t))v(t)^3 \right]} - \\ & \frac{\pi e_t \rho_l {C_{V_{t_l}}}^2 \left[tk(t,v(t))^2 v(t)^2 + \frac{cD^{1/6}}{{V_{i6}}^2} \left(\frac{C_{V_{t_l}}}{e_t} \right)^{1/2} t^{3/2} k(t,v(t))v(t)^4 \right]}{(m_p+m_l+m_f)v(t) + \pi e_t \rho_l {C_{V_{t_l}}}^2 \left[t^2 k(t,v(t))^2 v(t) + \frac{2cD^{1/6}}{{V_{i6}}^2} \left(\frac{C_{V_{t_l}}}{e_t} \right)^{1/2} t^{5/2} k(t,v(t))v(t)^3 \right]} \\ & x(0) = 0 \\ & v(0) = V_{i6} \end{aligned} \tag{52}$$

The following functions are defined to facilitate the handling of the equations which leads to Eq. (52):

$$h(t, v(t)) = \frac{dE_{TF}(t)}{dt} \frac{1}{v(t)} \tag{53}$$

$$g(t, x(t), v(t)) = \begin{cases} -\frac{d}{dt}[E_{DL}(t) + E_{MC}(t)], & \text{if } t \le \frac{\phi_p}{2C_{V_{t_l}}} \\ -\frac{d}{dt}[E_{ED}(t) + E_{DL}(t) + E_{MC}(t)], & \text{if } t > \frac{\phi_p}{2C_{V_{t_l}}} \end{cases} \tag{54}$$

$$k(t, v(t)) = cD^{1/6} \left(\frac{v(t)}{V_i} \right)^2 \left(\frac{C_{V_{t_l}} t}{e_t} \right)^{1/2}, k \in (0, 1] \tag{55}$$

This stage finishes when the parameter controlling the penetration process, $\delta(t)$, equals the laminate thickness:

$$\delta(t) = e_t \tag{56}$$

When Eq. (56) is met, the residual velocity is obtained.

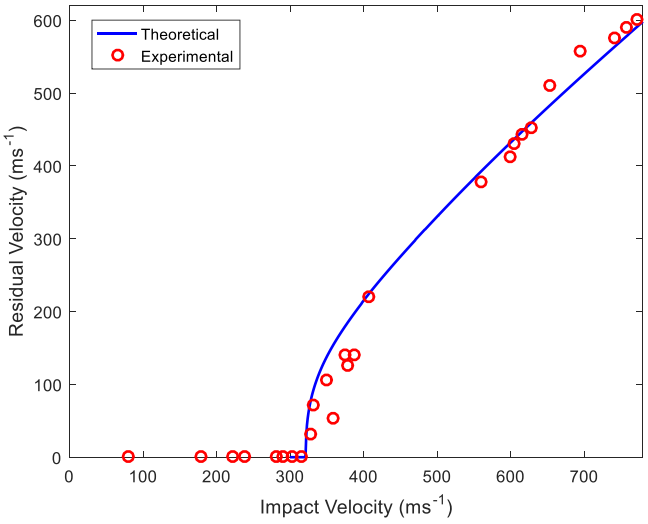

Fig. 5. Impact velocity versus residual velocity. Comparison between the results provided by the theoretical model presented and experimental data taken from the literature [27].

3. Verification and results

The aim of this section is, on the one hand, to validate the theoretical model by comparing against experimental results taken from previous literature studies. This comparison is carried out in the first subsection. On the other hand, two set of results regarding the impact process and the energy absorbed by the different energy-absorption mechanisms within each stage are obtained and properly discused in the second and third subsections.

3.1. Validation of the model

With validation purposes, we focus on the ballistic limit as the most important feature for the theoretical model to capture as well as the ballistic behaviour in terms of the impact velocity versus the residual velocity curve. In Fig. 5, the experimental impact velocity [27] versus the residual velocity curve is represented with circles and it is compared with those values (represented with a continuous line) obtained from the theoretical model proposed in the previous section.

As it can be seen, the results derived from the theoretical model proposed in this work present a good agreement with the experimental values. The ballistic limit predicted by the model is found to be 322 ms^{-1} while the experimental one [27] is 343 ms^{-1}. Therefore, the theoretical model provides a ballistic limit prediction with differences lower than 7% as well as a good fit to the high velocities range of the curve.

3.2. Study of the stage initial velocity of the projectile and stage duration times

Additionally, the initial velocities and duration times of each stage vs. impact velocity are shown in Fig. 6(a) and (b) respectively. These results allow to analyse the evolution of the penetration process in terms of the impact velocity.

In view of the results shown in Fig. 6(a), the energy absorbed in the first stage produces a mild decrease in the velocity (represented in the IV_{St2} curve) compared to the diminish that occurs in the linear momentum transfer in the second stage. This latter is represented in the IV_{St3} curve. Analogously, as it can be inferred from the fact that the IV_{St3}, IV_{St4} and IV_{St5} curves are coincident, no remarkable velocity decrease can be observed in the third and fourth stages. An important decrease can be appreciated in the last linear momentum transfer that takes place in the fifth stage, which is represented in terms of stage

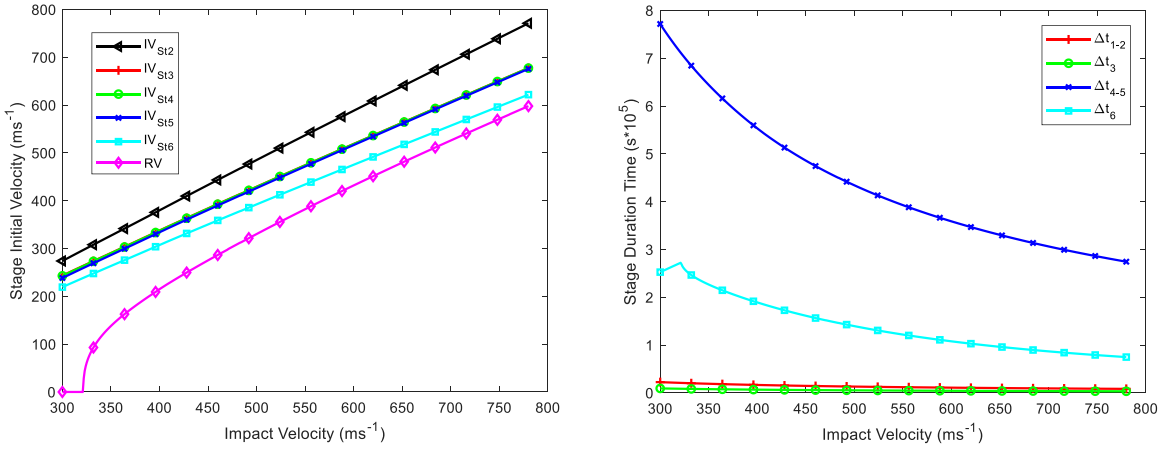

Fig. 6. (a) Impact velocity versus initial velocity in all stages within a velocity range from 300 m s^{-1} to 780 m s^{-1}, (b) Impact velocity versus stage duration time within a velocity range from 300 m s^{-1} to 780 m s^{-1}.

initial velocities in the IV_{St6} curve. If the initial projectile kinetic energy is low enough so that its value corresponds to a velocity under the ballistic limit, projectile and material plugs are always stopped in the rear facesheet, providing this last stage, the characteristic shape of the ballistic curve represented in Fig. 5 or in the RV curve in Fig. 6(a).

Furthermore, the behaviour of the curves shown in Fig. 6(b) reveals that the fourth stage ($\Delta t_{4\text{-}5}$ curve) is the longest process within the impact event. The duration times of the fourth and sixth stages may adopt values up to 80 μs and 30 μs respectively. The first and third stages[5] have a duration up to forty times shorter than the last ones becoming negligible in terms of time. The increasing impact velocity produces decreasing duration time curves for all stages as already shown in Fig. 6(b). This observation has a unique exception located in the lowest velocities of the Δt_6 curve. In this part, the time spent rises as the impact velocity increases until the ballistic limit is reached (point where the contact time is maximum), adopting a decreasing curve shape from this point on. The time of this stage increases as long as the penetration is longer before the ballistic limit. Once the ballistic limit has taken place, the resident time becomes shorter when increasing the impact velocity.

3.3. Study of the energy-absorption mechanisms by stage

The other set of results are related to the analysis of the energy-absorption mechanisms, which can be fundamental to understand the main failure and deformation mechanisms taking place during an impact. In Fig. 7 the energy-absorption mechanisms evolution with time are represented for all the stages (except for the instantaneous stages) for an impact velocity equal to the ballistic limit prediction provided by the theoretical model.

Fig. 7 (a) shows that the most important energy-absorption mechanisms are compression in region 1 and shear plugging. The great importance of these mechanisms is related to the thick behaviour assumed for the front peel, since no relevant bending is considered, compression and important shear stresses are generated leading to a plug formation in the second stage. Consequently, the failure assumed by compression in this stage is proven to be a good hypothesis. Fibre failure and kinetic energy transfer from the projectile to the laminate are secondary energy-absorption mechanisms. In addition, matrix cracking, delamination, compression in the foam and compression in region 2 play a minor role. Furthermore, a change in the slopes trend is observed in compression in region 1 and kinetic energy transfer from a time of 1.6 μs. This effect is a consequence of the through-thickness compression wave arrival to the foam. Since there is no more laminate material, the expressions described by Alonso et al. [3] for these mechanisms change to Eqs. (9) and (10). From this moment on, the foam starts absorbing energy by compression though is not perceptible in Fig. 7(a). Fig. 7(b) shows that the energy absorbed by the foam is negligible compared to the other stages. Within this stage the energy absorbed by shear is some orders of magnitude larger than compression. Therefore, the failure assumed by shear in this stage is reasonable. Fig. 7(c) represents the energy absorbed by densification in the fourth stage. The absorbed energy is linear with respect to time in this stage since the movement of the projectile is uniformly decelerated. Finally, Fig. 7(d) shows the evolution of the energy-absorption mechanisms in the sixth stage. This stage absorbs the most important amount of energy by far, being fibre failure the most important energy-absorption mechanism followed by elastic deformation of fibres. This result is in concordance with the thin laminates hypothesis assumed in this stage. Since there is an important bending of the rear peel, fibres are subjected to important tensile stresses and deformation leading to a failure of the fibre. Delamination, matrix cracking and kinetic energy transfer are proven to be minor energy-absorption mechanisms.

In order to see the change in the relative importance of the energy-absorption mechanisms with the impact velocity, the total energies absorbed by all the energy-absorption mechanisms are represented in Fig. 8 within a range of impact velocities from 80 ms^{-1} to 772 ms^{-1}, which are the limit experimental values available.

Fig. 8 (a) shows the final values of the energy-absorption mechanisms for different velocities in the first stage. It is interesting to analyse the change in trends of the mechanisms. In this regard, compression in both regions, shear plugging and fibre failure grow monotonously with impact velocity because the energy to absorb is higher and there is also more time until the projectile stops. This tendency changes when the laminate failure takes place, represented by the abrupt change in the energy curves. From that moment on, the contact time in the first stage decreases so there is less time to absorb energy (Fig. 6(b)). Consequently, fibre failure and compression in region 2 decrease. The latter reaches the value of zero when the initial velocity provokes an indentation of the projectile faster than the transverse wave in the laminate before complete failure. Kinetic energy transfer increases because the laminate ab-

[5] It is worth reminding that the second and fifth stages happen to be instantaneous as described above.

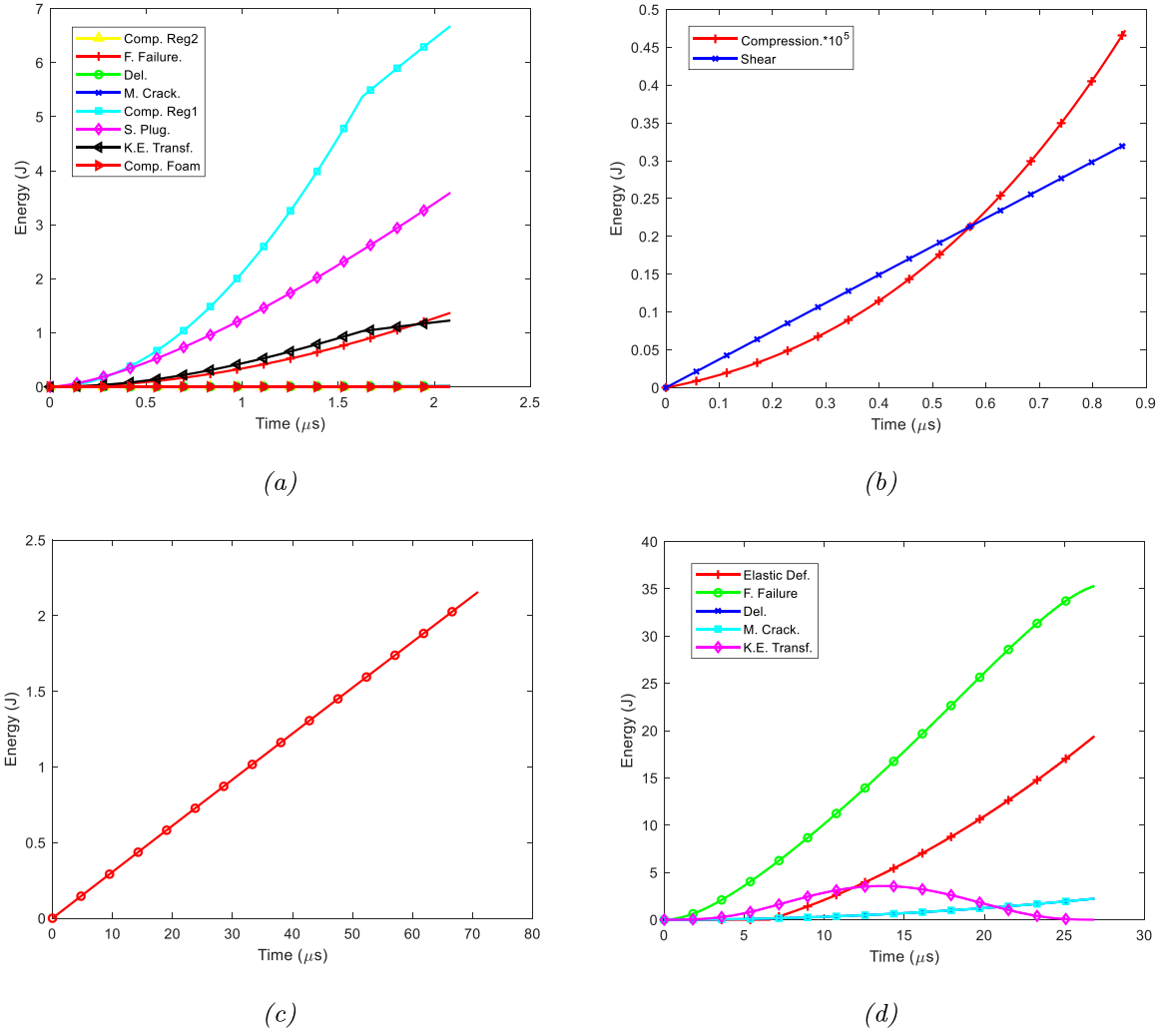

Fig. 7. Energy-absorption mechanisms evolution with respect to time for an impact velocity of 322 ms^{-1} with the initial time starting from 0 in all stages: (a) Stage 1 (b) Stage 3 (c) Stage 4 (d) Stage 6.

sorbs some kinetic energy from the projectile. Compression in region 1 and shear plugging remain constant because they reach their maximum value when there is perforation in the first peel. However, compression in region 1 starts decreasing when the initial velocity is high enough to provoke the laminate failure before the through-thickness wave reaches the last layer of the first peel, absorbing less energy by compression. The kinetic energy transfer changes its tendency too due to the change in the expression (Eq. (9)) explained by the previous fact. The other energy-absorption mechanisms play a minor role.

Fig. 8 (b) represents the energy lost by the projectile in the instantaneous kinetic energy transfer to the plug in the second stage. Since the velocity before the stage is linearly dependent of the velocity after the stage (Eq. (22)), the energy lost with respect to impact velocity presents a quadratics shape. Furthermore, this stage becomes the most important one for high velocities. Fig. 8(e) can be analysed in the same way. The only difference is the least absorbed-energy due to the fact that the foam density is an order of magnitude lower than the peels. Therefore, it takes less energy to move this plug than the plug in the second stage, leading to a less energy lost.

Fig. 8 (c) and (d) represent the stages related to the foam and as can be seen the total energy absorbed is really low in all cases. It can be inferred that the foam is not very relevant in the energy-absorption process. Fig. 8(c) shows that the energy absorbed by shear is by far more important than the energy absorbed by compression in the foam being both very small. Both energy-absorption mechanisms rise when full perforation of the first peel takes place. Since the energy absorbed is really low, energy absorbed by shear remains constant (because is the maximum value the foam can absorb) from that moment. Nevertheless, compression in the foam decreases with impact velocity because the projectile provokes the failure by shear before the through-thickness plastic wave travels through all the foam, absorbing less energy as long as the impact velocity increases.

Fig. 8 (f) shows the final values of the energy-absorption mechanisms for different velocities in the sixth stage. A growing trend is shown for all the mechanisms until full penetration except for the kinetic energy transfer. The more time the projectile interacts with the laminate the more energy absorbed. Nevertheless, since the laminate eventually stops if full penetration does not take place, the final value of the kinetic energy transfer is zero. The amount of energy absorbed by elastic deformation of fibres, fibre failure, delamination and matrix cracking decreases because there is less time to absorb energy. Since kinetic energy transfer is proportional to the projectile velocity and this latter is affected by the other energy-absorption mechanisms the trend of this mechanism presents a different shape. In general terms, the rear peel absorbs more energy than the front peel. Some energy-absorption mechanisms are more important as delamination and matrix cracking in the rear peel because the bending of the peel provokes important matrix breakage and layer debonding.

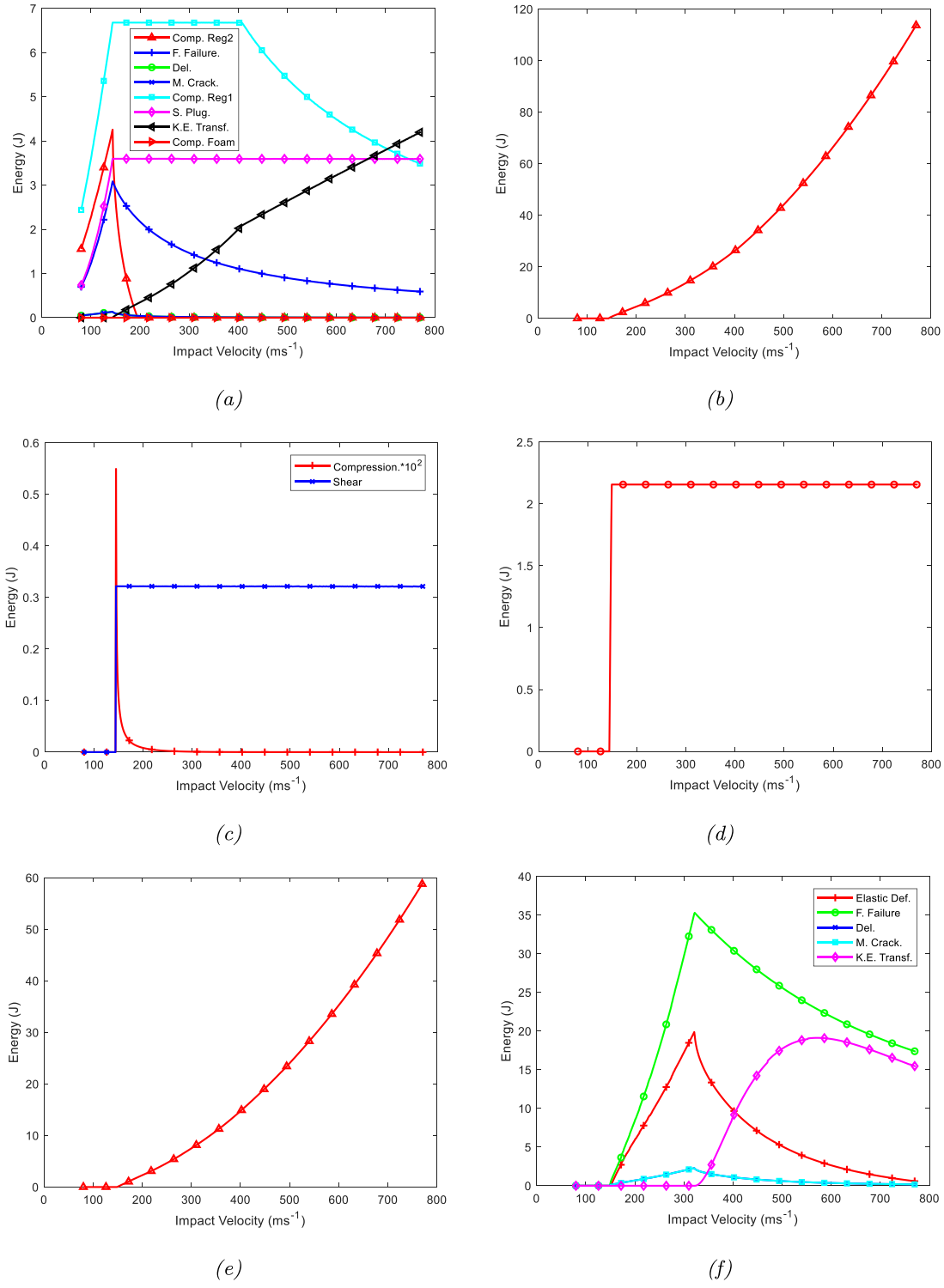

Fig. 8. Total energy absorbed versus impact velocity for all the energy-absorption mechanisms within a velocity range from 80 to 772 m s^{-1}: (a) Stage 1 (b) Stage 2 (c) Stage 3 (d) Stage 4 (e) Stage 5 (f) Stage 6.

4. Conclusions

In this work, a new energy-based theoretical model to analyse the performance of sandwich composite structures with PVC crushable foam core under high-velocity impact was proposed. The six stages considered were described by combining three different models based on the wave propagation theory. Two of them dealt with the front and rear peels of the sandwich assuming thick and thin woven laminates behaviour respectively. These considerations were made beforehand, supported in experimental observations and were proven analytically reasonable in view of the results obtained. Furthermore, the third stage was an original proposition to describe the projectile penetration through the foam core.

Additionally, a validation against experimental data was carried out in terms of the impact versus residual velocity curve, finding a good agreement regarding the ballistic limit and the values and trend of the curve. Different results such as the duration of the stages and the energy-

absorption mechanisms were analysed leading to the following conclusions:

- The ballistic response was accurately predicted within the whole velocity range, showing a ballistic limit error smaller than 7%.
- The major decrease in the projectile velocity took place in the rear laminate, followed by the ones produced in the instantaneous linear momentum transfers if the impact velocity was high enough. Nevertheless, the amount of energy lost by projectile was hardly noticeable in the foam stages.
- The forth and sixth stages were the most time spending ones. The time spent in the other stages was negligible in analytical terms.
- The most important energy-absorption mechanisms were the ones occurring in the sixth stage, especially fibre failure and elastic deformation of fibres. The energy absorbed in the remaining stages was two order of magnitude lower, having the compression in region 1 and shear plugging in the first stage the highest values. Moreover, kinetic energy transfer, fibre failure in the first stage, foam densification and shear plugging energy-absorption mechanisms played a secondary role. The energy absorbed in the foam due to plastic compression was negligible. All these conclusions correspond to the ballistic limit regime.
- The amount of energy absorbed by the most relevant energy-absorption mechanisms in the first stage increased as the projectile velocity approached to the failure condition. All the energy-absorption mechanisms affected by through-thickness wave decreased their importance when increasing the impact velocity because there was a point where the wave did not have time to cover all the peel/core distance. The reduction of kinetic energy experimented by the projectile in the instantaneous linear momentum transfers increased their importance with impact velocity becoming the most important for high-velocities. The energy absorbed by the foam was negligible within all the range of velocities. The last stage was the most important along with the kinetic energy transfers in terms of energy-absorbed. The behaviour of the energy-absorption mechanisms was the same than in the first stage. First, the energy absorbed rose until failure and then it diminished as the impact velocity increased. Energy absorbed by matrix cracking and delamination were more important in this stage compared to their values in the first stage since bending was considered.

Declaration of Competing Interest

The authors declare that they have no known competing financial interests or personal relationships that could have appeared to influence the work reported in this paper.

CRediT authorship contribution statement

L. Alonso: Conceptualization, Funding acquisition, Formal analysis, Data curation, Writing - original draft, Writing - review & editing, Validation. **A. Solis:** Conceptualization, Funding acquisition, Formal analysis, Data curation, Writing - original draft, Writing - review & editing, Validation.

References

[1] Abu Zahra N, Karimi S. On-line monitoring of pvc foam density using ultrasound waves and artificial neural networks. Int J Adv Manuf Technol 2002;19(8):618–22. doi:10.1007/s001700200067.

[2] Alonso L, Garcia-Gonzalez D, Martínez-Hergueta F, Navarro C, Teixeira-Dias F, García-Castillo S. Modeling high velocity impact on thin woven composite plates: a non-dimensional theoretical approach. Compos Part B 2021. doi:10.1080/15376494.2021.1878402.

[3] Alonso L, Garcia-Gonzalez D, Navarro C, García-Castillo S. A non-dimensional theoretical approach to model high-velocity impact on thick woven plates. Steel Compos Struct 2021. doi:10.12989/scs.2021.38.6.000.

[4] Alonso L, Navarro C, García-Castillo S. Analytical models for the perforation of thick and thin thicknesses woven-laminates subjected to high-velocity impact. Compos Part B 2018;143(15):292–300. doi:10.1016/j.compositesb.2018.01.030.

[5] Ansari M, Chakrabarti A, Iqbal M. An experimental and finite element investigation of the ballistic performance of laminated GFRP composite target. Compos Part B 2017;125:211–26. doi:10.1016/j.compositesb.2017.05.079.

[6] Briescani L, Manes A, Giglio M. An analytical model for ballistic impacts against plain-woven fabrics with a polymeric matrix. Int J Impact Eng 2015;78:138–49. doi:10.1016/j.ijimpeng.2015.01.001.

[7] Briesciani L, Manes A, Ruggiero A, Iannitti G, Giglio M. Experimental tests and numerical modelling of ballistic impacts against Kevlar 29 plain-woven fabrics with an epoxy matrix: macro-homogeneous and Meso-heterogeneous approaches. Compos Part B 2016;88:114–30. doi:10.1016/j.compositesb.2015.10.039.

[8] Buitrago B, García-Castillo S, Barbero E. Experimental analysis of perforation of glass/polyester structures subjected to high-velocity impact. Mater Lett 2010;64(9):1052–4. doi:10.1016/j.matlet.2010.02.007.

[9] Chu T, Ha-Minh C, Imad A. A numerical investigation of the influence of yarn mechanical and physical properties on the ballistic impact behavior of a Kevlar KM2® woven fabric. Compos Part B 2016;95(15):144–54. doi:10.1016/j.compositesb.2016.03.018.

[10] Costas M, Morin D, Langseth M, Díaz J, Romera L. Static crushing of aluminium tubes filled with pet foam and a GFRP skeleton. numerical modelling and multiobjective optimization. Int J Mech Sci 2017;131-132:205–17. doi:10.1016/j.ijmecsci.2017.07.004.

[11] D' Ottavio M, Vidal P, Valot E, Polit O. Assessment of plate theories for free-edge effects. Compos Part B 2013;48:111–21. doi:10.1016/j.compositesb.2012.12.007.

[12] Dhari R, Patel N, Wang H, Hazell P. Progressive damage modeling and optimization of fibrous composites under ballistic impact loading. Mech Adv Mater Struct 2019:1–18. doi:10.1080/15376494.2019.1655688.

[13] Ehsani A, Rezaeepazhand J. Stacking sequence optimization of laminated composite grid plates for maximum buckling load using genetic algorithm. Int J Mech Sci 2016;119:97–106. doi:10.1016/j.ijmecsci.2016.09.028.

[14] Feli S, Namdari-Pour M. An analytical model for composite sandwich panels with honeycomb core subjected to high-velocity impact. Compos Part B 2012;43(5):2439–47. doi:10.1016/j.compositesb.2011.11.028.

[15] García-Castillo S, Buitrago B, Barbero E. Behavior of sandwich structures and spaced plates subjected to highvelocity impacts. Polym Compos 2010. doi:10.1002/pc.21047.

[16] García-González D, Rusinek A, Jankowiak T, Arias A. Mechanical impact behaviour of polyether-ether-ketone (PEEK). Compos Struct 2015;124:88–99. doi:10.1016/j.compstruct.2014.12.061.

[17] Guangyong S, Tong S, Chen D, Gong Z, Li Q. Mechanical properties of hybrid composites reinforced by carbon and basalt fibers. Int J Mech Sci 2018;148:636–51. doi:10.1016/j.ijmecsci.2018.08.007.

[18] Hajikazemi M, Van Paepegem W. A variational model for free-edge interlaminar stress analysis in general symmetric and thin-ply composite laminates. Compos Struct 2018;184:443–51. doi:10.1016/j.compstruct.2017.10.012.

[19] Harding J, Ruiz C. The mechanical behaviour of composite materials under impact loading. Key Eng Mater 1998;141-143:403–26. doi:10.4028/www.scientific.net/KEM.141-143.403

[20] Harding J, Welsh L. A tensile testing technique for fiber-reinforced composites at impact rates of strain. J Mater Sci 1983;18:1810–26. doi:10.1007/BF00542078.

[21] Haro E, Odeshi A, Szpunar J. The energy absorption behavior of hybrid composite laminates containing nano-fillers under ballistic impact. Int J Impact Eng 2016;96:11–22. doi:10.1016/j.ijimpeng.2016.05.012.

[22] Hazzard M, Trask R, Heisserer U, Van Der Kamp M, Hallett S. Finite element modelling of Dyneema® composites: from quasi-static rates to ballistic impact. Compos Part A 2018;115:31–45. doi:10.1016/j.compositesa.2018.09.005.

[23] Heimbs S, Cichosz J, Klaus M, Kilchert S, Johnson A. Sandwich structures with textile-reinforced composite foldcores under impact loads. Compos Struct 2010;92(1):1485–97. doi:10.1016/j.compstruct.2009.11.001.

[24] Hongyong J, Yiru R, Binhua G, Jinwu X, Fu-Gwo Y. Design of novel plug-type triggers for composite square tubes: enhancement of energy-absorption capacity and inducing failure mechanisms. Int J Mech Sci 2017;113-136:636–51. doi:10.1016/j.ijmecsci.2017.06.050.

[25] Hoo Fatt M, Park K. Dynamic models for low-velocity impact damage of composite sandwich panels—Part a: Deformation. Compos Struct 2001;52(1):335–52. doi:10.1016/S1359-835X(00)00020-8.

[26] Hoo Fatt M, Sirivolu D. A wave propagation model for the high velocity impact response of a composite sandwich panel. Int J Impact Eng 2009;37(14):117–30. doi:10.1016/j.ijimpeng.2009.09.002.

[27] Iváñez I, Santiuste C, Barbero E, Sánchez-Sáez. Numerical modelling of foam-cored sandwich plates under high-velocity impact. Compos Struct 2011;93:2392–9. doi:10.1016/j.compstruct.2011.03.028.

[28] Iváñez I, Santiuste C, Sánchez-Sáez S. FEM analysis of dynamic flexural behaviour of composite sandwich beams with foam core. Compos Struct 2010;92(9):2285–91. doi:10.1016/j.compstruct.2009.07.018.

[29] Kharazan M, Sadr M, Kiani M. Delamination growth analysis in composite laminates subjected to low velocity impact. Steel Compos Struct 2014;17:387–403. doi:10.12989/scs.2014.17.4.387.

[30] Lei H, Yao K, Wen W, Zhou H, Fang D. Experimental and numerical investigation on the crushing behavior of sandwich composite under edgewise compression loading. Compos Part B 2016;94(1):34–44. doi:10.1016/j.compositesb.2016.03.049.

[31] Liu C, Zhang Y, Ye L. High velocity impact responses of sandwich panels with metal fibre laminate skins and aluminium foam core. Int J Impact Eng 2017(100):139–53. doi:10.1016/j.ijimpeng.2016.09.004.

[32] Maimí P, Camanho P, Mayugo J, Dávila C. A continuum damage model for composite laminates: Part ii-computational implementation and validation. Mech Mater 2007;39:909–19. doi:10.1016/j.mechmat.2007.03.006.
[33] Mamivand M, Liaghat G. A model for ballistic impact on multi-layer fabric targets. Int J Impact Eng 2010;37(7):806–12. doi:10.1016/j.ijimpeng.2010.01.003.
[34] Moure M, García-Castillo S, Sánchez-Sáez S, Barbero E, Barbero E. Influence of ply cluster thickness and location on matrix cracking evolution in open-hole composite laminates. Compos Part B 2016;95:40–7. doi:10.1016/j.compositesb.2016.03.091.
[35] Moyre S, Hine P, Duckett R, Carr D, Ward I. Modelling of the energy absorption by polymer composites upon ballistic impact. Compos Sci Technol 2000;60(14):2631–42. doi:10.1016/S0266-3538(00)00139-1.
[36] Naik N, Doshi A. Ballistic impact behaviour of thick composites: analytical formulation. AIAA J 2005;43(7):1525–36. doi:10.2514/1.11993.
[37] Naik N, Doshi A. Ballistic impact behaviour of thick composites:parametric studies. Compos Struct 2008;82(3):447–64. doi:10.1016/j.compstruct.2007.01.025.
[38] Naik N, Shrirao P. Composite structures under ballistic impact. Compos Struct 2004;66(1–4):579–90. doi:10.1016/j.compstruct.2004.05.006.
[39] Nasirzadeh R, Sabet A. Study of foam density variations in composite sandwich panels under high velocity impact loading. Int J Impact Eng 2014;63:129–39. doi:10.1016/j.ijimpeng.2013.08.009.
[40] Navarro C. Simplified modelling of the ballistic behaviour of fabric and fibre-reinforced polymer matrix composites. Key Eng Mater 1998;141-143:383–400.
[41] Parambil N, Gururaja S. Bridging micro-to-macro scale damage in UD-FRP laminates under tensile loading. Int J Mech Sci 2019;157-158:184–97. doi:10.1016/j.ijmecsci.2019.03.039.
[42] Qin Q-h, Zhang J-x, Wang Z-j, Li H-m, Dan G. Indentation of sandwich beams with metal foam core. Trans Nonferrous Metals Soc China 2014;24:2440–6. doi:10.1016/S1003-6326(14)63368-9.
[43] Ramadhan A, Abu Talib A, Mohd Rafie A, Zahari R. High velocity impact response of Kevlar-29/epoxy and 6061-T6 aluminum laminated panels. Mater Des 2013;43:307–21. doi:10.1016/j.matdes.2012.06.034.
[44] Reyes Villanueva G, Cantwell W. The high velocity impact response of composite and FML-reinforced sandwich structures. Compos Sci Technol 2004;4(1):35–54. doi:10.1016/S0266-3538(03)00197-0.
[45] Sangwook S, Sabyasachi G, Anderson D, Roy A. Enhancement of through-thickness thermal conductivity of sandwich construction using carbon foam. Compos Sci Technol 2012(72):767–73. https://doi.org/10.1016/j.compscitech.2012.02.003.
[46] Sikawar R, Velmurugan R, Gupta N. Influence of fiber orientation and thickness on the response of glass/epoxy composites subjected to impact loading. Compos Part B 2014;60:627–36. doi:10.1016/j.compositesb.2013.12.023.
[47] Silva M, Cisma C, Chiorean C. Numerical simulation of ballistic impact on composite laminates. Int J Impact Eng 2005;31(3):289–306. doi:10.1016/j.ijimpeng.2004.01.011.
[48] Smith J, FL M, Schiefer H. Stress-strain relationships in yarns subjected to rapid impact loading: 5. Wave propagation in long textile yarns impacted transversally. J Res Natl Bureau Stand 1958;60(5):517–34.
[49] Solis A, Sánchez-Sáez, Barbero E. Influence of ply orientation on free-edge effects in laminates subjected to in-plane loads. Compos Part B 2018;153:149–58. doi:10.1016/j.compositesb.2018.07.030.
[50] Stoll FC. Optimal design of sandwich core for wind turbine blade buckling resistance. American institute of aeronautics and astronautics 32nd ASME wind energy symposium; 2014. doi:102514/62014-0175.
[51] Su Z, Tay T, Ridha M, Chen B. Progressive damage modeling of open-hole composite laminates under compression. Compos Struct 2015;122:507–17. doi:10.1016/j.compstruct.2014.12.022.
[52] Tagarielli V, Deshpande V, Flecj N. The high strain rate response of PVC foams and end-grain balsa wood. Compos Part B 2008;39(1):83–91. doi:10.1016/j.compositesb.2007.02.005.
[53] Wang B, Zhang G, Wang S, Ma L, Wu L. High velocity impact response of composite lattice core sandwich structures. Appl Compos Mater 2017(21):377–89. doi:10.1007/s10443-013-9345-4.
[54] Zhang X, Liu T, He N, Jia G. Investigation of two finite element modelling approaches for ballistic impact response of composite laminates. Int J Crashrothiness 2016;22(4):377–93. doi:10.1080/13588265.2016.1270495.
[55] Zhu G, Sun G, Yu H, Li S, Li Q. Energy absorption of metal, composite and metal/composite hybrid structures under oblique crushing loading. Int J Mech Sci 2018;135:458–83. doi:10.1016/j.ijmecsci.2017.11.017.